Tailored MgAl Layered Double Hydroxide for Anionic Dye Removal from Aqueous Solution

Thanh-Linh Nguyen[1,2], Tuyet-Mai Tran-Thuy[1,2], and Minh-Kha Nguyen[1,2*]

[1]*Faculty of Chemical Engineering, Ho Chi Minh City University of Technology (HCMUT), 268 Ly Thuong Kiet St., Dien Hong Ward, Ho Chi Minh City 700000, Vietnam*

[2]*Vietnam National University Ho Chi Minh City, Linh Xuan Ward, Ho Chi Minh City 700000, Vietnam*

* ***Corresponding author:***

email: nmkha@hcmut.edu.vn

Received: September 1, 2025
Accepted: January 7, 2026

DOI: 10.22146/ijc.110854

Abstract: *The rapid growth of the textile dyeing industry has led to serious water pollution, with methyl orange (MO) being a persistent and hazardous azo dye. Adsorption is an effective and economical treatment method, and layered double hydroxides (LDHs) are promising adsorbents due to their tunable composition, high anion-exchange capacity, and structural versatility. However, the effect of synthesis parameters and competing interlayer anions on MO adsorption remains insufficiently understood. In this study, MgAl-LDH was synthesized by co-precipitation, and the influence of pH, Mg^{2+}/Al^{3+} molar ratio, aging time, and the presence of carbonate (CO_3^{2-}) or citrate ($C_6H_5O_7^{3-}$) ions was systematically examined. Operational factors, including solution pH, initial MO concentration, and contact time, were also evaluated. Optimal MO removal (>80%) was achieved at pH 9, an Mg^{2+}/Al^{3+} ratio of 3:1, a catalyst dosage of 0.2 g/L, and 24 h aging. In contrast, CO_3^{2-} and $C_6H_5O_7^{3-}$ incorporation disrupted the LDH structure, lowering adsorption efficiency. Isotherm analysis showed that the Sips model best described the adsorption process, reflecting both surface heterogeneity and site saturation. These findings highlight the critical role of synthesis conditions and interlayer anions, confirming MgAl-LDH as a robust and scalable adsorbent for anionic dye removal from wastewater.*

Keywords: *MgAl-LDH; layered double hydroxide; methyl orange removal; anionic dyes; wastewater treatment*

■ INTRODUCTION

Anionic dyes are a major class of persistent organic pollutants discharged in large volumes from textile, leather, paper, and related industries. Characterized by functional groups such as sulfonates, these dyes exhibit high water solubility, chemical stability, and strong resistance to biodegradation, enabling them to persist in aquatic environments long after discharge [1]. Their presence can severely impair water quality by reducing light penetration, disrupting photosynthetic activity, altering dissolved oxygen levels, and potentially introducing mutagenic or carcinogenic effects into ecosystems [2-3]. Among various anionic dyes, methyl orange (MO) serves as a widely recognized and challenging model pollutant. As an azo dye, MO is extensively applied in textile dyeing, leather finishing, and paper printing due to its vivid coloration, stability, and resistance to natural degradation [4]. These properties, while desirable in industrial applications, make MO particularly difficult to remove from wastewater, thereby underscoring the urgent need for effective treatment technologies targeting anionic dye pollutants [5].

Layered double hydroxides (LDHs), also known as hydrotalcite-like compounds or anionic clays, have attracted considerable attention as promising adsorbents for anionic species in aqueous systems [6]. They possess a general formula $M^{2+}_{1-x}M^{3+}_x(OH)_{2x}/_n{\cdot}mH_2O$, where M^{2+} and M^{3+} are divalent (e.g., Mg^{2+}, Zn^{2+}, Ni^{2+}) and trivalent (e.g., Al^{3+}, Fe^{3+}, Cr^{3+}) metal cations, respectively, and A^{n-} is an exchangeable interlayer anion (e.g., CO_3^{2-}, NO_3^-, PO_4^{3-}) [7]. Their positively charged brucite-like layers are balanced by interlayer anions and water molecules,

enabling high anion exchange capacity, tunable composition, and regeneration [8-10]. These properties make LDHs particularly suitable for removing anionic dyes, such as MO, via adsorption and ion-exchange mechanisms. Recent studies have demonstrated LDHs' high efficiency in removing anionic dyes like MO [11], Congo red [12], and tartrazine [13], yet adsorption performance strongly depends on synthesis parameters, interlayer anion type, and operational adsorption conditions.

Recent advances have focused on optimizing LDHs' synthesis to improve adsorption efficiency through parameters such as metal ions, precursor type, and crystallinity [14]. However, systematic studies linking synthesis variables to adsorption performance toward MO remain limited. In particular, the role of competing interlayer anions introduced during synthesis, especially their influence on LDHs' structural integrity, layer charge density, and active site accessibility, remains poorly understood [15]. Moreover, the combined effects of synthesis parameters and adsorption conditions on MO removal efficiency have not yet been comprehensively elucidated. Addressing these gaps is critical for developing robust, scalable LDH-based adsorbents capable of targeting MO and other anionic dyes under realistic wastewater conditions.

In this work, MgAl-LDH was synthesized via the co-precipitation method under carefully controlled conditions to remove MO from aqueous solutions. We systematically examined how synthesis conditions and interlayer anion type affect adsorption capacity, and how operational parameters such as pH, contact time, and initial dye concentration influence MO removal efficiency. This study offers new insights into optimizing LDH synthesis and application conditions for the efficient removal of anionic dyes from wastewater.

■ EXPERIMENTAL SECTION

Materials

All chemicals were of analytical grade and used without further purification. Magnesium nitrate hexahydrate ($Mg(NO_3)_2{\cdot}6H_2O$, >98%) and aluminum nitrate nonahydrate ($Al(NO_3)_3{\cdot}9H_2O$, >98%) were supplied by Oxford Lab Fine Chem LLP (India). Sodium carbonate (Na_2CO_3, >99%), sodium hydroxide (NaOH, >96%), trisodium citrate dihydrate ($Na_3C_6H_5O_7{\cdot}2H_2O$, >99%), and MO ($C_{14}H_{14}N_3NaO_3S$, >98%) were purchased from Xilong Scientific Co. (China). Deionized water was used throughout all experiments.

Instrumentation

The crystalline structure of the synthesized MgAl-LDH samples was analyzed by X-ray powder diffraction (XRD) using a Bruker D2 Phaser diffractometer (Germany) with Cu Kα radiation (λ = 1.54 Å) operated at 30 kV and 10 mA. The morphology was examined by field-emission scanning electron microscopy (FE-SEM, Hitachi S-4800). Nitrogen adsorption–desorption isotherms and specific surface areas were measured with a Nova e4000 analyzer (Quantachrome, USA). Prior to analysis, the MgAl-LDH sample was degassed under vacuum at 77 K for 6 h to remove adsorbed moisture and impurities, ensuring accurate BET surface area and pore structure characterization. Fourier-transform infrared (FTIR) spectra were recorded on a Frontier NIR/MIR spectrometer (PerkinElmer, USA) in the range of 400–4000 cm^{-1} using the KBr pellet method to identify surface functional groups and interlayer anions.

Procedure

Synthesis of MgAl-LDH

MgAl-LDH samples were synthesized using a previously reported co-precipitation method with several modifications [16]. Briefly, $Mg(NO_3)_2{\cdot}6H_2O$ and 1.25 g of $Al(NO_3)_3{\cdot}9H_2O$ were dissolved in 1 mL of deionized water. The amount of $Mg(NO_3)_2{\cdot}6H_2O$ was adjusted to achieve Mg^{2+}/Al^{3+} molar ratios ranging from 1:1 to 5:1. The pH of the solution was adjusted to values between 7 and 11 by dropwise addition of 0.3 M NaOH under continuous magnetic stirring and maintained for 30 min to ensure complete precipitation. The resulting suspension was aged at room temperature (~28 °C) for 8–48 h. To investigate the effect of interlayer anions, CO_3^{2-} or citrate ($C_6H_5O_7^{3-}$) ions were introduced during synthesis by varying the molar ratio of Na_2CO_3 or $Na_3C_6H_5O_7$ to NaOH. The precipitate was recovered by vacuum filtration, thoroughly washed with deionized water to remove residual ions, and dried at 80 °C for 8 h.

The dried powders were stored in sealed glass vials until use.

To determine the optimal synthesis conditions for MO adsorption, the MgAl-LDH sample exhibiting the highest removal efficiency was first identified through preliminary adsorption tests. Based on this, the influence of key synthesis parameters was systematically investigated, including the Mg^{2+}/Al^{3+} molar ratio, initial solution pH, and aging time. Additionally, the effect of interlayer anion type was examined by introducing CO_3^{2-} or $C_6H_5O_7^{3-}$ ions during synthesis. For this purpose, the molar ratio of Na_2CO_3 or $Na_3C_6H_5O_7$ to NaOH was varied to evaluate how these anions affected the structural formation and subsequent adsorption capacity of MgAl-LDH.

Study of MO adsorption

To evaluate the adsorption efficiency for MO removal, each MgAl-LDH sample synthesized under the respective experimental conditions was tested using a catalyst dosage of 0.2 g L^{-1} in 50 mL of MO solution with an initial concentration of 200 mg L^{-1}. The mixture was agitated at 300 rpm for 90 min at room temperature. After adsorption, the suspension was filtered through 0.45 μm membrane filters. The residual MO concentration was determined using a UV-vis spectrophotometer at 464 nm. All experiments were conducted in duplicate to ensure reproducibility. The MO adsorption capacity (q_t, mg/g) at time t was calculated using Eq. (1):

$$q_t = \frac{(C_0 - C_t)V}{m} \quad (1)$$

where C_0 and C_t (mg/L) are the initial and time t concentrations of MO in solution, respectively, V (L) is the solution volume, and m (g) is the adsorbent mass.

The optimized MgAl-LDH sample was used to assess the influence of operational parameters, including solution pH, contact time, adsorbent dosage, and initial MO concentration, on adsorption performance. The kinetic models applied for MO adsorption onto MgAl–LDH are presented in Table 1, while the isotherm models employed in this study are summarized in Table 2.

■ RESULTS AND DISCUSSION

Influence of MgAl-LDH Synthesis Conditions on MO Removal

Effect of Mg^{2+}/Al^{3+} molar ratio on LDH synthesis

XRD patterns in Fig. 1(a) confirmed that the hydrotalcite structure was stably maintained across Mg/Al ratios from 2:1 to 5:1 (JCPDS card no. 00-014-0191). Characteristic reflections at (003), (006), (009), and (110) were clearly observed, indicating robust LDH formation without secondary phases such as $Mg(OH)_2$, MgO, or Al_2O_3, which are often reported at high Mg/Al ratios [17]. Peak (003) showed systematic shifts in interlayer spacing with varying Mg/Al ratios, reflecting changes in layer charge density. The peak around 30° observed in some samples may be related to the presence of nitrate-containing Mg–Al LDH phases [18], where NO_3^- serves as the interlayer anion. During synthesis, NO_3^-–LDH can readily exchange anions with CO_3^{2-}, leading to structural variations that may influence diffraction features. These variations directly affect electrostatic interactions with intercalated anions, influencing anion exchange and adsorption capacity. The high phase purity confirms that the adsorption performance can be attributed solely to the LDH phase.

The MgAl-LDH synthesized at a Mg^{2+}/Al^{3+} molar ratio of 3:1 exhibited the highest MO removal efficiency (~77%, Fig. 1(b)), with both efficiency and adsorption

Table 1. Kinetic models applied for MO adsorption onto MgAl–LDH

Model	Nonlinear expression	Linear form
Pseudo-first-order (PFO)	$q_t = q_e\left(1 - e^{-k_1 t}\right)$	$\ln(q_e - q_t) = \ln(q_e) - k_1 t$
Pseudo-second-order (PSO)	$q_t = \frac{q_e^2 k_2 t}{1 + q_e k_2 t}$	$\frac{t}{q_t} = \frac{1}{k_2 q_e^2} + \frac{t}{q_e}$

where q_t and q_e were the amounts of MO adsorbed (mg/g) at time t (min) and at equilibrium, respectively, and k_1 and k_2 are the pseudo-first-order and pseudo-second-order rate constants (g/mg min)

Table 2. Isotherm models applied for MO adsorption onto MgAl–LDH

Model	Nonlinear expression	Linear form
Langmuir	$q_e = \frac{q_m K_L C_e}{1 + K_L C_e}$	$\frac{1}{q_e} = \frac{1}{C_e K_L q_m} + \frac{1}{q_m}$
Freundlich	$q_e = K_F C_e^{1/n}$	$\ln q_e = \ln K_F + \frac{1}{n} \ln C_e$
Temkin	$q_e = \frac{RT}{b_T} \ln(A_T C_e)$	$q_e = \frac{RT}{b_T} \ln A_T + \frac{RT}{b_T} \ln C_e$
Sips	$q_e = \frac{q_m K_S C_e^n}{1 + K_S C_e^n}$	$\ln\left(\frac{q_e}{q_m - q_e}\right) = n \ln C_e + \ln K_S$

where C_e is the equilibrium concentration of MO in solution (mg/L), q_e is the equilibrium adsorption capacity (mg/g), q_m is the maximum monolayer adsorption capacity (mg/g), K_L is the Langmuir constant (L/mg); K_F is the Freundlich constants, and n is a heterogeneity factor in adsorption; A_T is Temkin equilibrium binding constant (L/g), R is ideal gas constant (J/mol K), T is temperature (K) and b_T is Temkin constant related to adsorption heat (J/mol); and K_S is the Sips isotherm constant (L/mg)^n

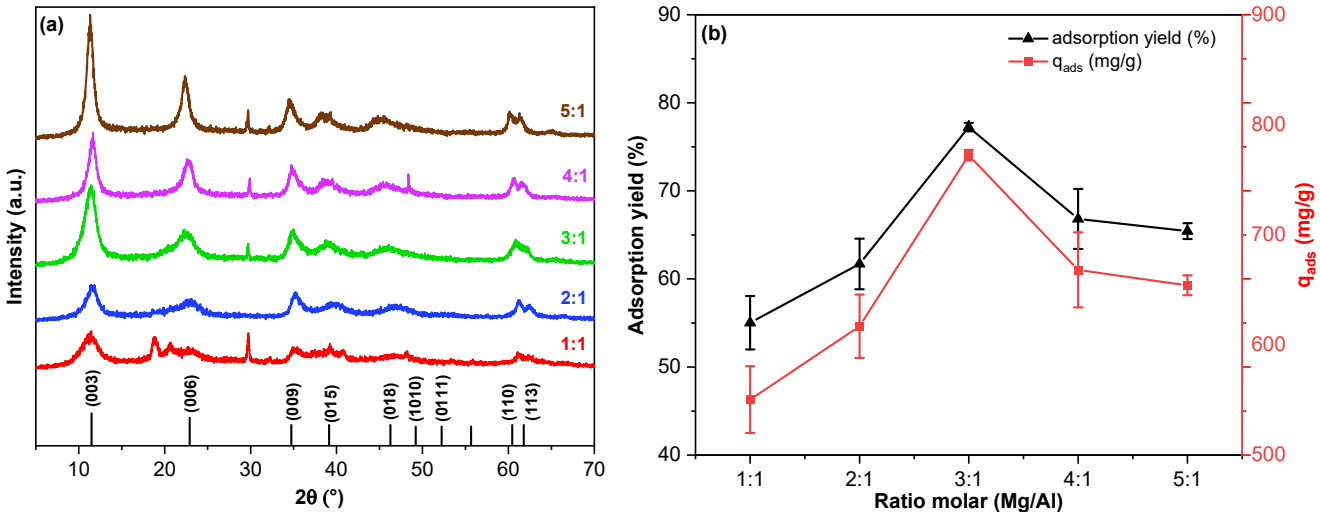

Fig 1. Effect of Mg^{2+}/Al^{3+} molar ratio on MgAl-LDH properties: (a) XRD patterns and (b) MO adsorption

capacity increasing from 1:1 to 3:1, then declining at higher ratios. This volcano-shaped trend indicates that neither Mg-rich nor Al-rich compositions are optimal; instead, adsorption performance depends on a balance between electrostatic attraction and structural stability. XRD analysis provides direct evidence for this behavior: samples with Mg^{2+}/Al^{3+} molar ratios of 1:1 and 2:1 showed broad, weak peaks, suggesting poor crystallinity and structural disorder that hinder adsorption, whereas at 3:1 sharp, intense peaks confirmed improved crystallinity, enhanced interlayer ordering, and stable charge exchange for MO anions. In contrast, excess Mg at 4:1 and 5:1 produced peak broadening and lattice defects, reducing layer charge density and adsorption capacity [19-20]. The Mg^{2+}/Al^{3+} molar ratio of 3:1, with sufficient cations in the LDH structure to sustain a strong positive layer charge, achieved an adsorption capacity of ~770 mg/g, highlighting its superiority over Mg-rich or Al-rich LDHs previously reported [21-23]. Overall, the findings demonstrate that the Mg/Al ratio critically governs both structural features and adsorption yield, with the 3:1 ratio providing optimum crystallinity and charge balance.

Effect of pH on LDH synthesis

The XRD patterns in Fig. 2(a) show that synthesis pH strongly influences the crystallinity of MgAl-LDH,

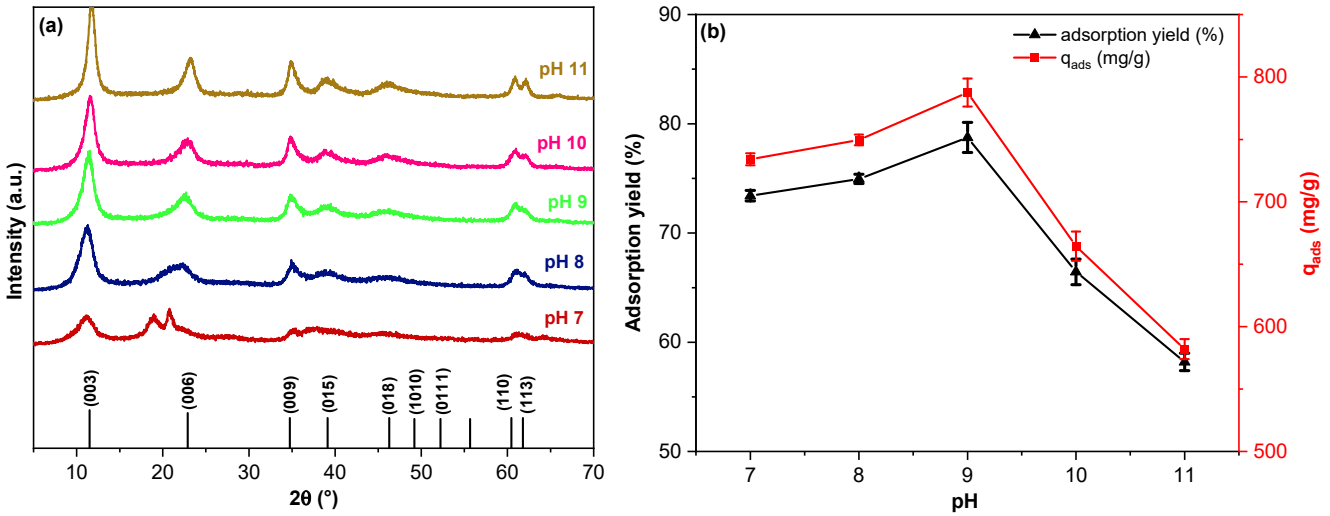

Fig 2. Effect of pH on MgAl-LDH properties: (a) XRD patterns and (b) MO adsorption

which directly correlates with adsorption performance (Fig. 2(b)). At pH 7, broad and weak peaks indicate poorly crystalline LDH, consistent with low adsorption efficiency due to limited structural order. Increasing the pH to 8 slightly improves crystallinity and adsorption capacity, while the optimum occurs at pH 9, where sharp and intense peaks confirm high crystallinity and well-ordered interlayers [24-25]. This structural quality provides abundant, uniform adsorption sites and enables superior MO removal efficiency. At higher pH values (10–11), adsorption performance decreases sharply because rapid precipitation creates lattice defects and secondary phases such as isolated hydroxides that block active sites [26]. All samples retained characteristic LDH reflections, particularly the (003), (006), and (009) planes, confirming the layered structure. The direct correlation between synthesis pH, crystallinity, and adsorption yield confirms that pH 9 is the optimal condition for tailoring LDH-based adsorbents.

Effect of aging time on LDH synthesis

The effect of aging time on the crystallinity and adsorption performance of MgAl-LDH is shown in Fig. 3. Samples aged between 8 and 24 h exhibited progressive improvement in crystallinity, as indicated by sharper XRD peaks, which directly correlated with higher MO adsorption capacity. Optimum performance

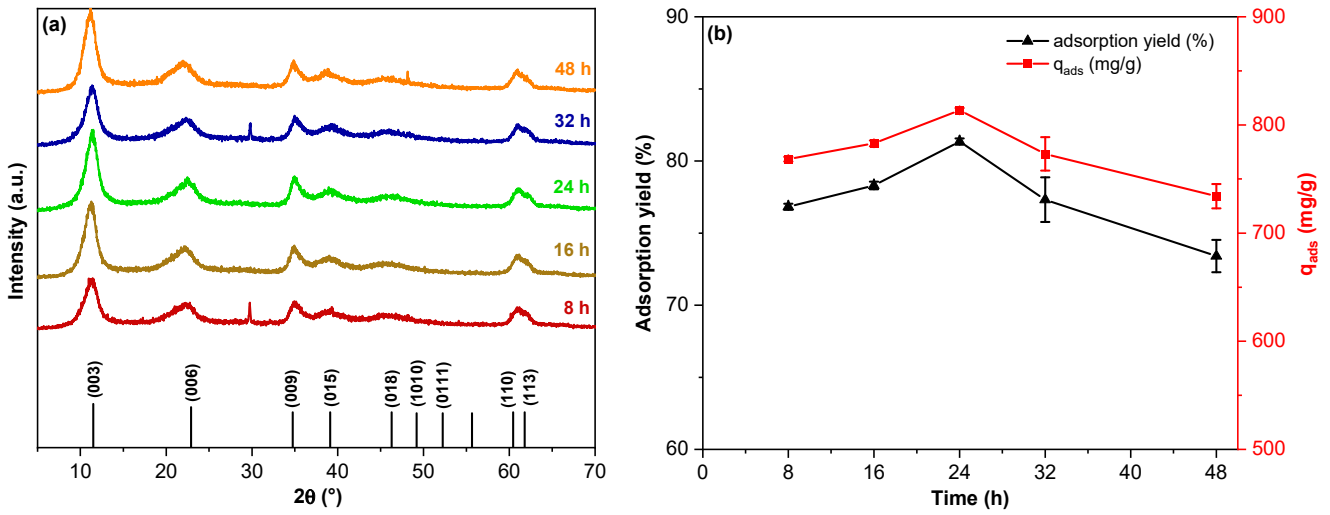

Fig 3. Effect of aging time on MgAl-LDH properties: (a) XRD patterns and (b) MO adsorption

was observed at 24 h, when improved stacking order and larger crystallite size provided a stable structure with abundant active sites [27]. However, extending the aging time to 32 and 48 h led to a decline in both crystallinity and adsorption yield, likely due to the emergence of amorphous phases and defect accumulation, which reduced the effective surface area. Interestingly, the interlayer anions and hydration state remained unchanged across all samples, confirming that the differences in performance may originate primarily from crystallinity, stacking order, and defect density [28]. This finding contrasts with prior assumptions that longer aging universally improves performance revealing that excessive aging diminishes adsorption capacity [29]. Overall, these results establish aging time as a critical synthesis parameter, demonstrating that 24 h of aging maximizes both crystallinity and functional performance.

Effect of competing anions on LDH synthesis

Ions with different sizes, charge densities, and coordination abilities can alter interlayer spacing, layer stacking, and adsorption behavior. XRD patterns and adsorption yield in Fig. 4 reveal distinct effects of anions on the structure of MgAl-LDH. The CO_3^{2-} ions correlate with sharper, more intense peaks (Fig. 4(a)), reflecting strong interlayer incorporation [30], which severely reduces MO adsorption. In contrast, $C_6H_5O_7^{3-}$ ions induce interlayer expansion and peak broadening due to their competition with the host layers, yet still allow partial recovery of adsorption at higher concentrations. This integrated structure–property analysis provides a new perspective on anion competition, a key factor for translating LDH adsorption studies from idealized to realistic water environments [31]. The CO_3^{2-}, abundant in natural waters, shows a strong affinity for LDH-CO_3

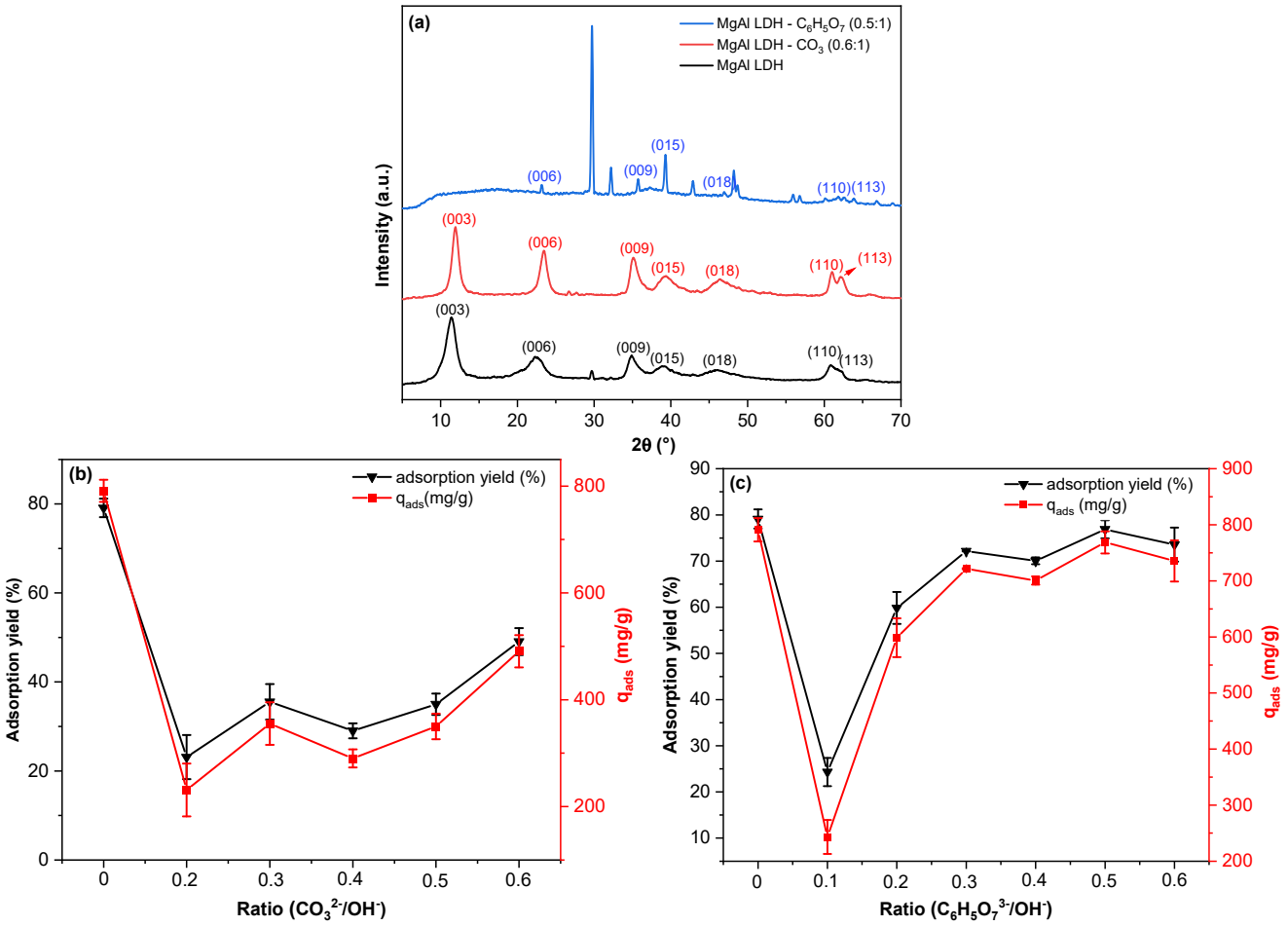

Fig 4. Effect of competing anions on MgAl-LDH properties: (a) XRD patterns, (b) effect of LDH-CO_3 on MO adsorption; (b) effect of LDH-$C_6H_5O_7$ on MO adsorption

interlayers, making it a major inhibitor of dye removal. The $C_6H_5O_7^{3-}$, representing organic anions from natural degradation, competes mainly via surface chelation and partial intercalation [32], leading to milder inhibition. Interestingly, when the $C_6H_5O_7^{3-}/OH^-$ ratio increased from 0.1 to 0.5, adsorption of LDH-$C_6H_5O_7$ did not decrease monotonically; instead, steric hindrance and electrostatic repulsion partially limited $C_6H_5O_7^{3-}$ competition, allowing higher MO uptake. Together, these results establish that CO_3^{2-} strongly blocks interlayer exchange [30], while $C_6H_5O_7^{3-}$'s weaker and reversible interaction leaves adsorption pathways partially accessible. Such insights are important for evaluating LDH performance in complex aqueous systems and highlight conditions where MgAl-LDH remains viable for dye removal.

Characterization of Synthesized MgAl-LDH

SEM image (Fig. 5(a)) of MgAl–LDH synthesized under the optimum conditions (pH 9, Mg^{2+}/Al^{3+} ratio of 3:1, without competing anions, and 24 h aging) showed uniform particles. The average particle size, estimated from SEM images using ImageJ across multiple regions, was ~94 nm. FTIR spectra (Fig. 5(b)) confirmed the presence of hydroxyl groups and interlayer water, with broad O–H stretching bands at 3400–3500 cm^{-1} and bending vibrations at 1638 cm^{-1} [33]. Both pure MgAl-LDH and carbonate-intercalated samples exhibited a sharp band at 1384 cm^{-1}, characteristic of CO_3^{2-} ions commonly incorporated during synthesis [34]. In contrast, the MgAl-LDH–citrate sample displayed additional peaks at 1283 and 1077 cm^{-1} [35-36], confirming successful intercalation of bulky $C_6H_5O_7^{3-}$ ions

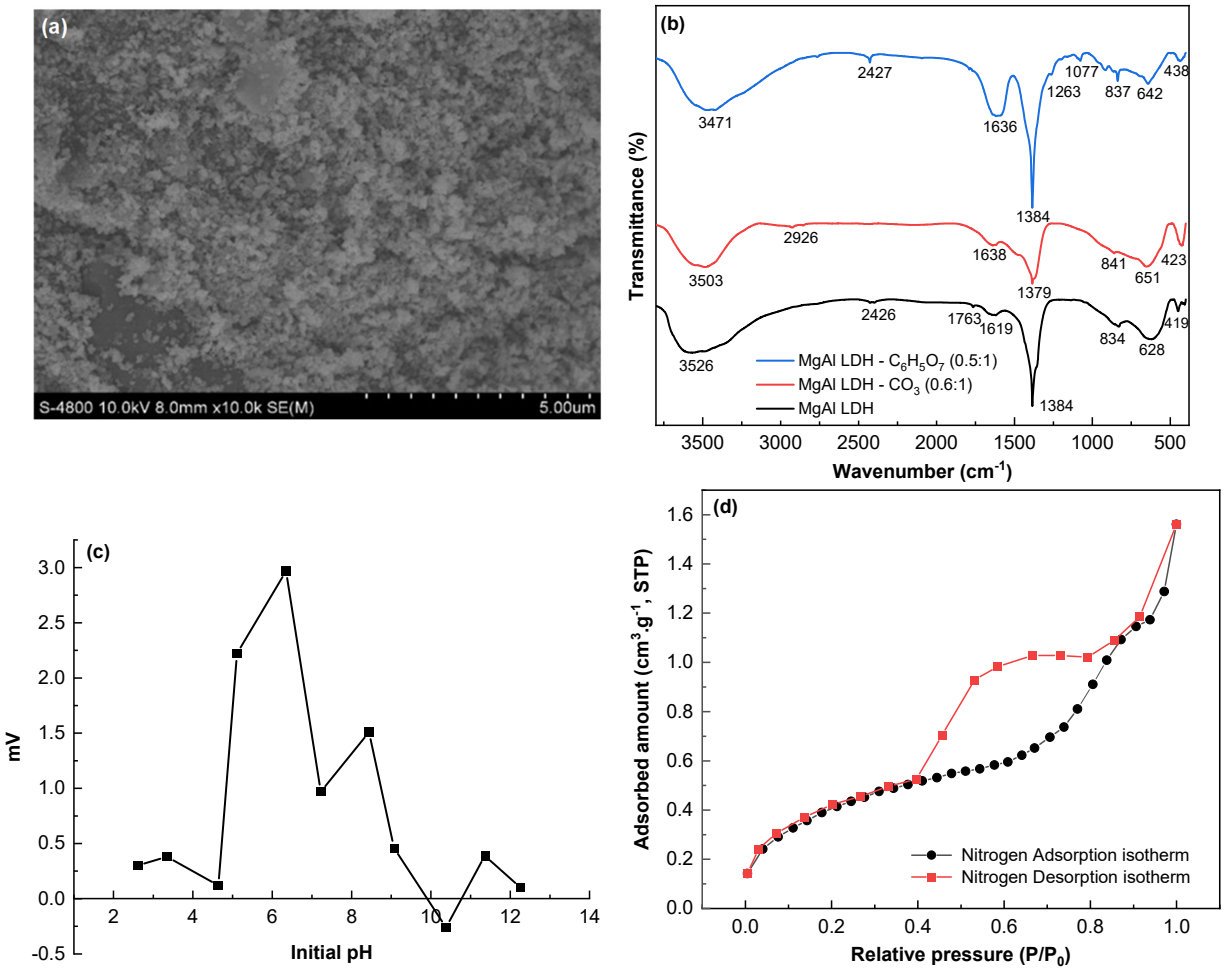

Fig 5. Characterization of MgAl-LDH: (a) SEM image, (b) FTIR spectra, (c) isoelectric point diagram, and (d) N_2 adsorption-desorption isotherms

despite steric and electrostatic constraints. The isoelectric point (Fig. 5(c)) was ~10, indicating a positively charged surface below this pH, which favors anion adsorption [37]. Anionic dye adsorption occurs mainly via electrostatic attraction between the LDH surface and dye anions, and partial anion exchange at OH-rich edge sites where interlayer anions (e.g., CO_3^{2-}) are replaced by dye anions. The N_2 adsorption–desorption isotherms (Fig. 5(d)) exhibited a type H3 hysteresis loop, typical of slit-shaped pores in LDH aggregates [38]. Despite the low BET surface area (1.6 m^2/g), effective MO removal suggests that ion exchange dominates the adsorption mechanism [39-41].

Adsorption Efficiency MO of MgAl-LDH

Effect of contact time and kinetic study

Fig. 6(a) shows the effect of contact time on MO adsorption by MgAl–LDH. Removal efficiency increased rapidly during the first 1 h (≈70%), then slowed and reached equilibrium at ~3 h. The adsorption capacity followed the same trend, rising sharply to ~750 mg/g before stabilizing ~820 mg/g. This two-stage behavior suggests an initial surface adsorption phase, followed by slower uptake controlled by site saturation or intraparticle diffusion [42]. The fast initial uptake is attributed to abundant active sites, while the subsequent slowdown reflects electrostatic repulsion between adsorbed MO molecules. Kinetic fitting (Fig. 6(b-c)) showed that the PSO model best described the data, indicating chemisorption via electron exchange between MO anions and the positively charged LDH layers. In contrast, the PFO model showed poor agreement, confirming that physisorption is not dominant. These results align with previous studies highlighting electrostatic interactions

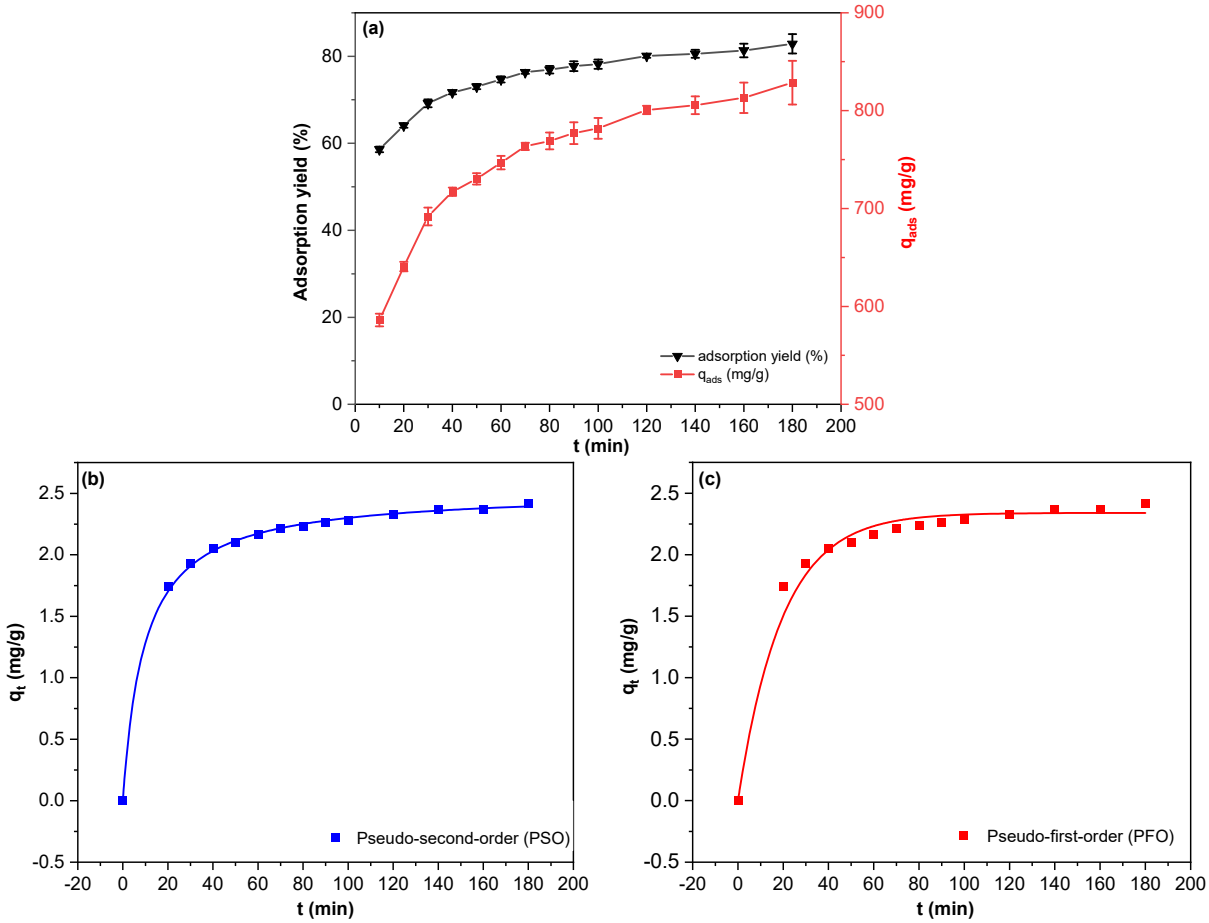

Fig 6. (a) Effect of contact time on the adsorption of MO onto MgAl–LDH (C_0 = 200 ppm, adsorbent dosage = 0.2 g/L), and (b) kinetic model fitting of the adsorption data using PSO and (c) PFO

and surface complexation as key mechanisms in LDH-based dye adsorption [43].

Effect of pH and adsorbent dosage on MO adsorption

The adsorption of MO by MgAl-LDH was strongly affected by solution pH and adsorbent dosage. As shown in Fig. 7(a), the adsorption yield increased from pH 6 to 9, reaching ~80%, due to reduced electrostatic repulsion between MO anions and partially deprotonated OH groups on the LDH surface. At higher pH (10–11), both yield and capacity declined, likely because of competition with OH^- ions and weakened electrostatic attraction. This trend agrees with previous reports on LDH-based adsorbents [44]. The effect of adsorbent dosage (Fig. 7(b)) showed that increasing MgAl-LDH from 0.1 to 1.2 g/L enhanced removal efficiency, reaching ~98% at the highest dosage, owing to the greater number of available adsorption sites. However, the adsorption capacity per unit mass decreased with dosage, which can be attributed to particle aggregation and less efficient use of active sites, a phenomenon commonly observed in adsorption systems.

Effect of initial MO concentrations and adsorption isotherms

Fig. 8 showed that the initial MO concentration (C_0) strongly influenced adsorption by MgAl-LDH. As C_0 increased from 25 to 300 ppm, the adsorption capacity rose from ~50 to >1000 mg/g due to a higher concentration gradient and greater availability of MO molecules for interaction with active sites. However, the adsorption yield displayed a different trend: it remained above 80% at 25 ppm, but declined to ~44% between 50–75 ppm, and increased to 300 ppm. This decrease is attributed to surface saturation, where the number of MO molecules exceeds available adsorption sites [45-46]. As the concentration increased to 75 ppm, the adsorption yield decreased due to partial surface saturation of active sites and increased competition among dye anions. At higher initial concentrations (100–250 ppm), the yield gradually increased and stabilized around 70–80%, suggesting the involvement of additional adsorption mechanisms such as interlayer

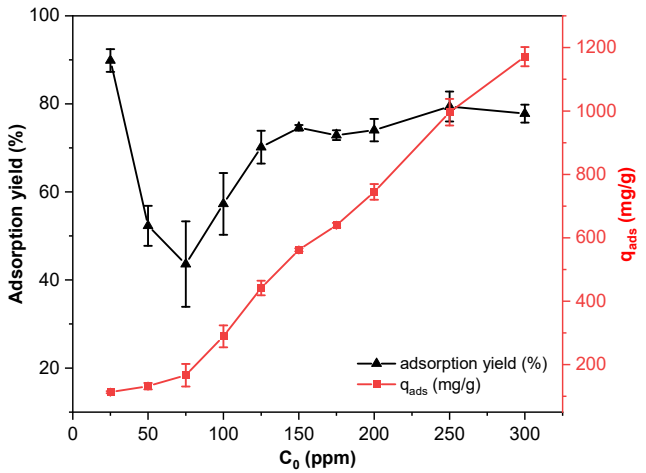

Fig 8. Effect of initial MO concentration on the adsorption of MO onto MgAl–LDH (adsorbent dosage = 0.2 g/L)

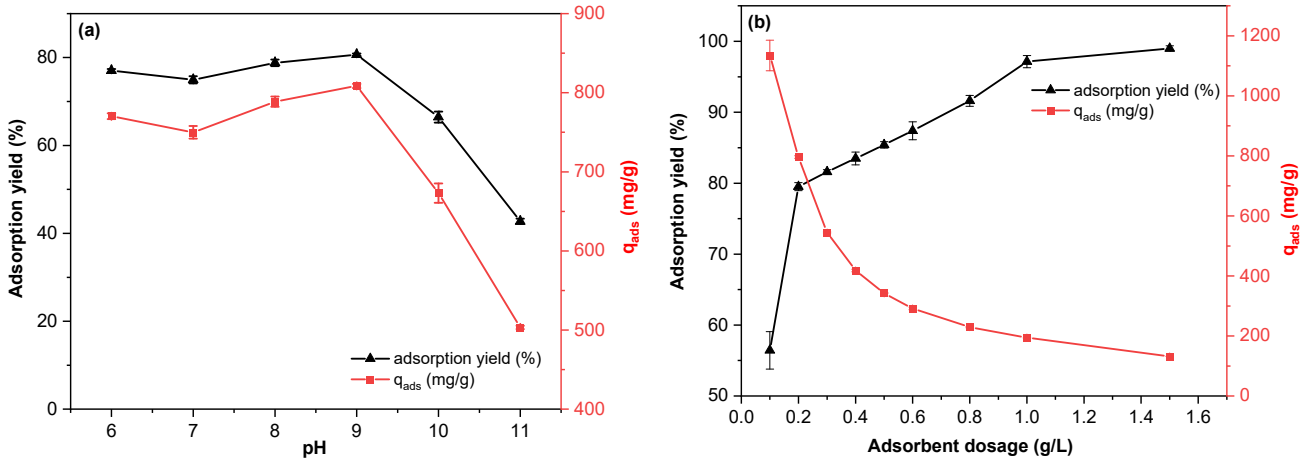

Fig 7. (a) Effect of pH in adsorption of 200 ppm MO and an adsorbent dosage of 0.2 g/L; and (b) effect of adsorbent dosage in adsorption of MO

anion exchange and electrostatic interactions. Meanwhile, the adsorption capacity increased continuously with increasing initial concentration, from approximately 140 mg/g at 25 ppm MO to about 1200 mg/g at 300 ppm MO, driven by the higher concentration gradient. These results indicate that although surface site saturation reduced the adsorption yield, the MgAl-LDH exhibited a high adsorption capacity for MO, with optimal performance observed around 250 ppm. This behavior highlights the strong affinity of the material for MO and emphasizes the importance of balancing adsorption capacity and efficiency in practical wastewater treatment applications.

Equilibrium adsorption of MO onto MgAl-LDH was investigated at an adsorbent dosage of 0.2 g/L and various initial concentrations, with adsorption isotherms fitted to Langmuir, Freundlich, Temkin, and Sips models (Fig. 9), and the results are summarized in Table 3. The initial dye concentration reflects the adsorption process and reveals the interactions between adsorbent and adsorbate. The fitting parameters and correlation coefficients are summarized in Table 3. The Langmuir model (Fig. 9(a)) showed slight deviation at higher equilibrium concentrations due to its assumption of uniform adsorption sites. Nevertheless, it fitted the experimental data well (R^2 = 0.9774), indicating predominantly monolayer adsorption behavior. The high maximum adsorption capacity is attributed to strong electrostatic attraction and anion-exchange interactions between MO anions and the positively charged MgAl-LDH layers. The Freundlich model also gave a strong correlation (R^2 = 0.9915, Fig. 9(b)), with an

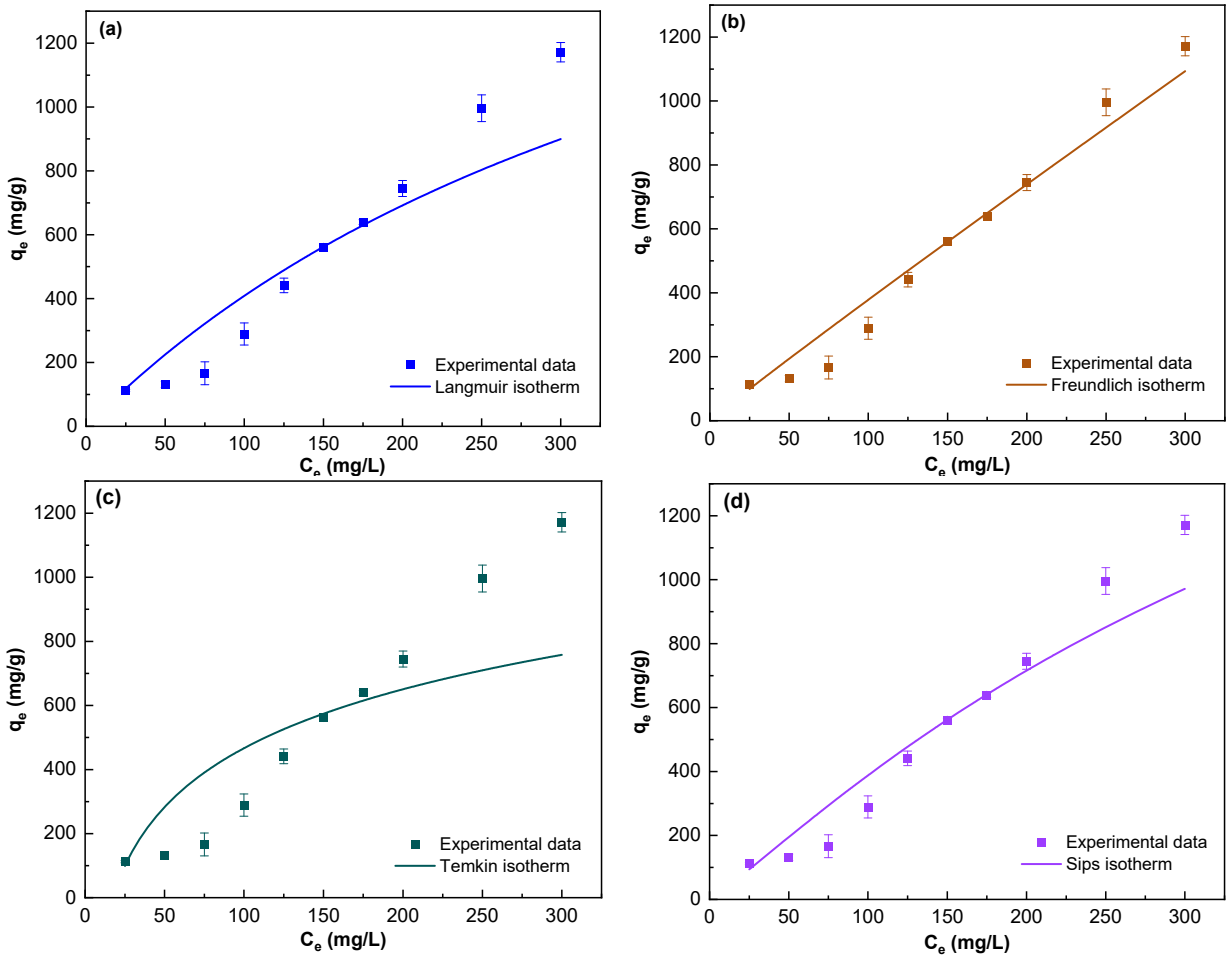

Fig 9. Adsorption isotherms of MO onto MgAl–LDH (adsorbent dosage = 0.2 g/L) fitted with the (a) Langmuir, (b) Freundlich, (c) Temkin, and (d) Sips models

Table 3. Isotherm fitting parameters for MO adsorption onto MgAl-LDH

Model	Parameter	Fitting value
Langmuir	q_m (mg/g)	2248.2947
	K_L (L/mg)	0.0022
	R^2	0.9774
Freundlich	K_F (L/mg)	4.4190
	n	1.0349
	R^2	0.9915
Temkin	b_T (J.g/mol.mg)	265.1320
	A_T (L/mg)	0.0581
	R^2	0.9429
Sips	q_m (mg/g)	2595.3307
	K_S (L/mg)	0.0021
	n	1.1147
	R^2	0.9850

n value of 1.0349, indicating favorable adsorption and surface heterogeneity [47]. In contrast, the Temkin model (Fig. 9(c)) was less suitable for describing the adsorption behavior because it assumes a linear energy distribution [48]. The Sips isotherm also showed good agreement with the experimental data (R^2 = 0.9850, Fig. 9(d)), confirming its ability to describe adsorption on heterogeneous surfaces at high concentrations while approaching Langmuir-type monolayer adsorption at lower concentrations [49]. Although the Freundlich model exhibited the highest correlation coefficient (R^2 = 0.9915), the Sips model remains more appropriate as it accounts for both surface heterogeneity and maximum adsorption capacity, which are important at higher MO concentrations. The positively charged MgAl-LDH surface promotes strong electrostatic attraction with the negatively charged sulfonate groups of MO, while partial anion exchange between interlayer CO_3^{2-} and MO^- further enhances adsorption. Additionally, surface OH groups may form hydrogen bonds with MO molecules. These combined effects, i.e., electrostatic attraction, anion exchange, and hydrogen bonding, explain the high adsorption capacity and strong affinity of MO toward MgAl-LDH. Overall, the results suggest that MO adsorption onto MgAl-LDH involves both surface heterogeneity and adsorption site saturation.

■ CONCLUSION

In this study, MgAl-LDH was successfully synthesized via co-precipitation and its structure and morphology were confirmed by XRD, SEM, and FTIR analyses. SEM images revealed a flake-like structure, while the interlayer spacing of the LDH was closely related to its adsorption affinity. The optimized conditions for MO removal were identified as an initial concentration of 250 ppm, a Mg/Al molar ratio of 3:1, pH 9, aging time of 24 h, and adsorbent dosage of 0.2 g/L, considering the influence of CO_3^{2-} and $C_6H_5O_7^{3-}$ ions during synthesis. Under these conditions, over 80% decolorization efficiency was achieved within 90 min. MO adsorption onto MgAl-LDH involves both surface heterogeneity and adsorption site saturation. The results indicate that MgAl-LDH is an effective adsorbent for the removal of high-concentration anionic dyes from wastewater, with significant potential for practical applications in water treatment.

■ ACKNOWLEDGMENTS

We acknowledge Ho Chi Minh City University of Technology (HCMUT), VNU-HCM, for supporting this study.

■ CONFLICT OF INTEREST

The authors declare that there are no conflicts of interest regarding the publication of this paper.

■ AUTHOR CONTRIBUTIONS

Thanh-Linh Nguyen performed the experiments, conducted the data analysis, and wrote the manuscript. Tuyet-Mai Tran-Thuy contributed to methodology and validation. Minh-Kha Nguyen contributed to conceptualization, methodology, data analysis, and manuscript editing. All authors reviewed and approved the final version of the manuscript.

■ REFERENCES

[1] Amalina, F., Abd Razak, A.S., Krishnan, S., Zularisam, A.W., and Nasrullah, M., 2022, Dyes removal from textile wastewater by agricultural

waste as an absorbent – A review, *Cleaner Waste Syst.*, 3, 100051.

[2] Al-Tohamy, R., Ali, S.S., Li, F., Okasha, K.M., Mahmoud, Y.A.G., Elsamahy, T., Jiao, H., Fu, Y., and Sun, J., 2022, A critical review on the treatment of dye-containing wastewater: Ecotoxicological and health concerns of textile dyes and possible remediation approaches for environmental safety, *Ecotoxicol. Environ. Saf.*, 231, 113160.

[3] Nguyen, K.M., Pham, N.N., Tran, H.T.T., and Nguyen, S.T., 2025, Dual-functional Fe_3O_4@SiO_2/Ag/AgCl nanocomposites as photocatalyst for degrading methylene blue dye under natural light irradiation, *Indones. J. Chem.*, 25 (1), 169–177.

[4] Pranta, A.D., and Rahaman, M.T., 2024, Extraction of eco-friendly natural dyes and biomordants for textile coloration: A critical review, *Nano-Struct. Nano-Objects*, 39, 101243.

[5] Worku, A.K., Ayele, D.W., Teshager, M.A., Omar, M., Yerkrang, P.P., Elgaddafi, R., and Alemu, M.A., 2025, Recent advances in wastewater treatment technologies: Innovations and new insights, *Energy Rev.*, 4 (4), 100164.

[6] Farhan, A., Khalid, A., Maqsood, N., Iftekhar, S., Sharif, H.M.A., Qi, F., Sillanpää, M., and Asif, M.B., 2024, Progress in layered double hydroxides (LDHs): Synthesis and application in adsorption, catalysis and photoreduction, *Sci. Total Environ.*, 912, 169160.

[7] Wang, P., Zhang, X., Zhou, B., Meng, F., Wang, Y., and Wen, G., 2023, Recent advance of layered double hydroxides materials: Structure, properties, synthesis, modification and applications of wastewater treatment, *J. Environ. Chem. Eng.*, 11 (6), 111191.

[8] Zaghloul, A., Benhiti, R., Ait Ichou, A., Carja, G., Soudani, A., Zerbet, M., Sinan, F., and Chiban, M., 2021, Characterization and application of MgAl layered double hydroxide for methyl orange removal from aqueous solution, *Mater. Today: Proc.*, 37, 3793–3797.

[9] Tabish, M., Tabinda, A.B., Mazhar, Z., Yasar, A., Ansar, J., and Wasif, I., 2024, Physical, chemical and biological treatment of textile wastewater for removal of dyes and heavy metals, *Desalin. Water Treat.*, 320, 100842.

[10] Sharma, R., Arizaga, G.G.C., Saini, A.K., and Shandilya, P., 2021, Layered double hydroxide as multifunctional materials for environmental remediation: From chemical pollutants to microorganisms, *Sustainable Mater.Technol.*, 29, e00319.

[11] Bokka, S., Singh, R., and Chowdhury, A., 2024, Efficacy of Mg-Al-layered double hydroxide nano-adsorbents for a multi-anionic mixed dye solution, *J. Mol. Liq.*, 396, 123984.

[12] Sun, W., Liu, C., Liu, S., Zhang, J., Chen, H., and Qiu, Z., 2025, Effective adsorption of Congo red by an innovative biochar/LDH-derived MIL-100(Al): Investigation of coexisting pollutants and mechanism revelation, *Sep. Purif. Technol.*, 359, 130670.

[13] Jamhour, R.M.A.Q., Al-Msiedeen, A.M., Al-Sharaydeh, R.Z., Jamhour, M.R., and Altweiq, A.M., 2024, Zn-Al layered double hydroxide nanoparticles for efficient removal of food dyes from wastewater, *Desalin. Water Treat.*, 317, 100036.

[14] Lee, S.Y., Choi, J.W., Song, K.G., Choi, K., Lee, Y.J., and Jung, K.W., 2019, Adsorption and mechanistic study for phosphate removal by rice husk-derived biochar functionalized with Mg/Al-calcined layered double hydroxides via co-pyrolysis, *Composites, Part B*, 176, 107209.

[15] Xu, Y., Huang, W., Chen, X., Ge, F., Zhu, R., and Sun, L., 2018, Self-assembled ZnAl-LDH/PMo_{12} nano-hybrids as effective catalysts on the degradation of methyl orange under room temperature and ambient pressure, *Appl. Catal., A*, 550, 206–213.

[16] Yuan, D., Zhou, L., and Fu, D., 2017, Adsorption of methyl orange from aqueous solutions by calcined ZnMgAl hydrotalcite, *Appl. Phys. A: Mater. Sci. Process.*, 123 (2), 146.

[17] Pettauer, M., Baldermann, A., Eder, S., and Dietzel, M., 2024, Hydration of MgO: Reaction kinetics and

pH control on brucite crystal morphology, *Cryst. Growth Des.*, 24 (7), 3085–3092.

[18] Huang, G., Ma, S., Zhao, X., Yang, X., and Ooi, K., 2009, Topotactic intercalation of a bulky organic anion (thiacalix[4]arene) into LDH through an osmotic swelling/restoration reaction in formamide, *Chem. Commun.*, 3, 331–333.

[19] Bing, X., Li, J., Liu, J., Cui, X., and Ji, F., 2018, Biomimetic synthesis of Bi_2O_3/Bi_2WO_6/MgAl-CLDH hybrids from lotus pollen and their enhanced adsorption and photocatalysis performance, *J. Photochem. Photobiol., A*, 364, 449–460.

[20] Rybka, K., Matusik, J., and Marzec, M., 2022, Mg/Al and Mg/Fe layered double hydroxides derived from magnesite and chemicals: The effect of adsorbent features and anions chemistry on their removal efficiency, *J. Cleaner Prod.*, 332, 130084.

[21] Qin, J., Shi, H., Lv, Q., He, M., Xu, Y., Chen, M., Chen, X., Zhang, J., Liu, Y., and Yu, J., 2023, Enhanced adsorption effect of defect ordering Mg/Al on layered double hydroxides nanosheets with highly efficient removal of Congo red, *Mater. Des.*, 232, 112084.

[22] Wang, S.L., Liu, C.H., Wang, M.K., Chuang, Y.H., and Chiang, P.N., 2009, Arsenate adsorption by Mg/Al–NO_3 layered double hydroxides with varying the Mg/Al ratio, *Appl. Clay Sci.*, 43 (1), 79–85.

[23] Johnston, A.L., Lester, E., Williams, O., and Gomes, R.L., 2021, Understanding layered double hydroxide properties as sorbent materials for removing organic pollutants from environmental waters, *J. Environ. Chem. Eng.*, 9 (4), 105197.

[24] Mureseanu, M., Eliescu, A., Ignat, E.C., Carja, G., and Cioatera, N., 2022, Different routes of MgAl–LDH synthesis for tailoring the adsorption of Pb(II) pollutant from water, *C. R. Chim.*, 25, 281–292.

[25] Zubair, M., Daud, M., McKay, G., Shehzad, F., and Al-Harthi, M.A., 2017, Recent progress in layered double hydroxides (LDH)-containing hybrids as adsorbents for water remediation, *Appl. Clay Sci.*, 143, 279–292.

[26] Altalhi, A.A., Mohamed, E.A., and Negm, N.A., 2024, Recent advances in layered double hydroxide (LDH)-based materials: Fabrication, modification strategies, characterization, promising environmental catalytic applications, and prospective aspects, *Energy Adv.*, 3 (9), 2136–2151.

[27] Feng, L., Li, A., Li, Y., Liu, J., Wang, L., Huang, L., Wang, Y., and Ge, X., 2017, A highly active CoFe layered double hydroxide for water splitting, *ChemPlusChem*, 82 (3), 483–488.

[28] Bhojaraj, B., and Rajamathi, M., 2023, Anion exchange reactions of $3R_2$-MgAl-carbonate-LDH: Comparison with the $3R_1$ analogue and formation of $3R_2$ polytype of MgAl-LDH with other interlayer anions, *ACS Omega*, 8 (11), 10185–10190.

[29] Chen, Y., Jing, C., Zhang, X., Jiang, D., Liu, X., Dong, B., Feng, L., Li, S., and Zhang, Y., 2019, Acid-salt treated CoAl layered double hydroxide nanosheets with enhanced adsorption capacity of methyl orange dye, *J. Colloid Interface Sci.*, 548, 100–109.

[30] Rahmanian, O., Dinari, M., and Neamati, S., 2018, Synthesis and characterization of citrate intercalated layered double hydroxide as a green adsorbent for Ni^{2+} and Pb^{2+} removal, *Environ. Sci. Pollut. Res.*, 25 (36), 36267–36277.

[31] Shan, Z., Feng, K., Du, L., Liu, X., Lu, H., Wang, S., Wang, W., and Guo, F., 2025, Selective capture and co-removal of anionic dyes with multi-metallic nanosheets: Superior properties and multi-sites synergistic mechanism, *J. Water Process Eng.*, 74, 107797.

[32] Wieszczycka, K., Staszak, K., Woźniak-Budych, M.J., Litowczenko, J., Maciejewska, B.M., and Jurga, S., 2021, Surface functionalization – The way for advanced applications of smart materials, *Coord. Chem. Rev.*, 436, 213846.

[33] Lu, Y., Wang, X., Xu, X., Wu, P., Li, Z., and Zhang, G., 2025, Hierarchically structured CoAl-LDH derived hybrid membrane for synergistic solar-driven water purification and photocatalytic CO_2 reduction, *Desalination*, 613, 118992.

[34] Dang, L., Liang, H., Zhuo, J., Lamb, B.K., Sheng, H., Yang, Y., and Jin, S., 2018, Direct synthesis and anion exchange of noncarbonate-intercalated

NiFe-layered double hydroxides and the influence on electrocatalysis, *Chem. Mater.*, 30 (13), 4321–4330.

[35] Zhang, B., Dong, Z., Sun, D., Wu, T., and Li, Y., 2017, Enhanced adsorption capacity of dyes by surfactant-modified layered double hydroxides from aqueous solution, *J. Ind. Eng. Chem.*, 49, 208–218.

[36] Yuan, L., Wang, C., Qing, X., Bi, M., Huang, G., and Weng, X., 2020, Synthesis and fine spectroscopy tuning of the hyperspectral simulation material based on organic anions intercalated Mg-Al layered double hydroxide, *Infrared Phys. Technol.*, 107, 103328.

[37] Jia, Y.H., and Liu, Z.H., 2019, Preparation of borate anions intercalated MgAl-LDHs microsphere and its calcinated product with superior adsorption performance for Congo red, *Colloids Surf., A*, 575, 373–381.

[38] Stepanova, L.N., Belskaya, O.B., Salanov, A.N., Serkova, A.N., and Likholobov, V.A., 2018, SEM study of the surface morphology and chemical composition of the MgAl- and MgGa-layered hydroxides in different steps of platinum catalysts Pt/Mg(Al, Ga)O_x synthesis, *Appl. Clay Sci.*, 157, 267–273.

[39] Munnik, P., de Jongh, P.E., and de Jong, K.P., 2015, Recent developments in the synthesis of supported catalysts, *Chem. Rev.*, 115 (14), 6687–6718.

[40] Nguyen, M.K., Nguyen, T.C.A., and Vo, Q.A., 2024, Actual adsorptive efficiency of aqueous Cr(VI) using modified banana pseudostems, *IOP Conf. Ser.: Earth Environ. Sci.*, 1340 (1), 012015.

[41] Tao, X., Liu, D., Cong, W., and Huang, L., 2018, Controllable synthesis of starch-modified ZnMgAl-LDHs for adsorption property improvement, *Appl. Surf. Sci.*, 457, 572–579.

[42] Rashed, S.H., Abd-Elhamid, A.I., Abdalkarim, S.Y.H., El-Sayed, R.H., El-Bardan, A.A., Soliman, H.M.A., and Nayl, A.A., 2022, Preparation and characterization of layered-double hydroxides decorated on graphene oxide for dye removal from aqueous solution, *J. Mater. Res. Technol.*, 17, 2782–2795.

[43] Massrour, A., Peighambardoust, S.J., Foroughi, M., Foroutan, R., and Ramavandi, B., 2025, Crystal violet removal by sodium alginate-g-polyacrylamide/hydroxyapatite/Cu-Fe LDH nanocomposite, *Environ. Technol. Innovation*, 38, 104149.

[44] Wu, X., Xu, Y., Wang, J., Wen, Y., Wu, J., Wang, X., Wu, J., and Hao, C., 2025, Calcined COF-LDH adsorbent with memory effect: Enhanced removal of anionic and cationic dyes from wastewater, *Desalination*, 615, 119229.

[45] Salami, O.S., Sihlahla, M., Dladla, B.S., and Mketo, N., 2026, Adsorptive removal of additive potent organic toxicants from beverages and contaminated waters: A critical review of adsorbent materials, kinetics, isotherms, thermodynamics, mechanisms, and future prospects, *Sep. Purif. Technol.*, 380, 135453.

[46] Ko, S.J., Yamaguchi, T., Salles, F., and Oh, J.M., 2021, Systematic utilization of layered double hydroxide nanosheets for effective removal of methyl orange from an aqueous system by π-π stacking-induced nanoconfinement, *J. Environ. Manage.*, 277, 111455.

[47] Alotaibi, A.M., and Elsayed, N.H., 2025, Adsorption and eliminating of diquat herbicide using layer double hydroxide enclosed in double layer hydrogel beads of carboxymethyl cellulose and alginate: Synthesis, characterization, adsorption isotherm, kinetics, thermodynamics and optimization via Box-Behnken design, *Int. J. Biol. Macromol.*, 303, 140564.

[48] Lu, C., Han, X., Zou, H., Gao, X., and Wang, S., 2025, Adsorption of ciprofloxacin on (Zn-Al) LDHs modified 3D reduced graphene oxide: Response surface methodology, adsorption equilibrium, kinetic and thermodynamic studies, *Chin. J. Chem. Eng.*, 83, 125–136.

[49] Liu, B., Qin, L., and Cao, H., 2025, Nitrogen adsorption characteristics and specific heat capacities of two activated carbons for sorption-based compression, *Cryogenics*, 148, 104069.